

Mechanical properties of SiC nanowires determined by scanning electron and field emission microscopies

S. Perisanu,¹ V. Gouttenoire,¹ P. Vincent,^{1,*} A. Ayari,¹ M. Choueib,^{1,2} M. Bechelany,² D. Cornu,² and S. T. Purcell¹

¹*Laboratoire de Physique de la Matière Condensée et Nanostructures, Université Lyon 1, CNRS, UMR 5586, Domaine Scientifique de la Doua, F-69622 Villeurbanne Cedex, France*

²*Laboratoire Multimatériaux et Interfaces, Université Lyon 1, CNRS, UMR 5615, Domaine Scientifique de la Doua, F-69622 Villeurbanne Cedex, France*

(Received 19 December 2007; revised manuscript received 19 March 2008; published 30 April 2008)

We present here comparative measurements by scanning electron microscopy (SEM) and field emission (FE) of the mechanical resonances of singly clamped, batch-fabricated SiC nanowires as well as an extensive theoretical description. The mechanical resonances of six nanowires, which were glued to the ends of tungsten support tips, were electrostatically excited and detected visually in the SEM configuration and then by FE microscopy image processing. The large tensions generated by electric field pulling in FE that tune the resonance frequencies and the complex boundary conditions at both the free and clamped nanowire ends complicate the interpretation of the resonance frequencies necessary for extracting intrinsic mechanical parameters. Our model fully takes into account these effects and results in an excellent agreement with the measured resonance modes in both configurations. Analytical solutions with their validity conditions are given for the low and high tension ranges and semianalytical solutions for the intermediary range. Viable estimates of Young's modulus are thus achieved for the ultra high vacuum (UHV) environment of FE. Progressive *in situ* cleaning was performed in the FE-UHV configuration in the range of 600–1350 K, which increased the Q factor of the first mechanical resonance by up to $\times 100$ and did not alter the value of the Young's modulus measured previously in the SEM configuration. The agreement between the SEM and FE techniques means that we can now profit from their different strengths for better understanding the mechanics of nanowires and nanotubes.

DOI: [10.1103/PhysRevB.77.165434](https://doi.org/10.1103/PhysRevB.77.165434)

PACS number(s): 61.46.-w, 79.70.+q, 73.63.Fg

I. INTRODUCTION

The increasing attraction of researchers for nanoelectromechanical systems (NEMS) springs from the fact that their extremely small dimensions make them highly sensitive to external perturbations. As well their mechanical response can exceed the quality of electrical signals from purely electronic devices. The Q factor of macroscopic electronic oscillators is rather poor (at most a few hundreds) and it becomes even worse at the nanometric scale [Fig. 1(d) in Ref. 1]. Mechanical oscillators have Q factors up to 10^9 at macroscopic scale² and up to 10^5 at nanometric scale.^{3,4} This sensitivity has created potential applications for them as mass sensors, actuators, frequency filters or multipliers, etc., and makes them excellent systems for both fundamental physics and new nanodevices.⁵ The study of the basic mechanical phenomena in NEMS and how they can be best controlled by external parameters is of prime importance in order to exploit their possibilities in devices especially because new effects come into play at the nanoscale that lead to both complications and opportunities.

There are two categories of parameters that determine the behavior of the NEMS. First, the parameters related to the nanoresonator itself: Young's modulus, dimensions, density, and Q factor due to intrinsic energy dissipation. Second, the parameters related to the environment of the resonator inside the system, such as the electrical capacitance, the boundary conditions of the NEMS movement within its environment, and nonintrinsic energy loss mechanisms, such as nonperfect contacts, Foucault currents, adsorption, and mechanical or

electromagnetical radiation. These two types of parameters define the eigenfrequencies of the system, their tunability by mechanical stress (for example, due to electrostatic forces created by an applied voltage V_A), the widths of the resonances, the threshold between linear and nonlinear response to external excitation, etc.

NEMS that use mobile cantilevers mostly come in two standard configurations: doubly and singly clamped. The doubly clamped configuration has been more intensively studied both experimentally and theoretically.⁶⁻⁹ Examples of recent achievements are the realization of doubly clamped carbon nanotube (CNT) NEMS with detection by a single electron transistor,⁶ operating at frequencies up to 1.3 (Ref. 7) and 3.1 GHz (Ref. 8) with Q factors at most ≈ 100 .⁹ Theoretical models of this configuration have been realized,¹⁰ showing different ranges of frequency tuning by the applied voltage. The influence of slack in the doubly clamped configuration was also fully discussed by Üstünel *et al.* (Ref. 11); they explained the apparition of supplementary eigenmodes in this geometry.

The singly clamped configuration has been used to characterize the mechanical parameters of nanotubes¹² and nanowires¹³ by transmission electron microscopy (TEM) or scanning electron microscopy (SEM) and is explored for applications in CNT switches both theoretically and experimentally.¹⁵ This configuration is also ideal for field emission microscopy (FEM) measurements of the mechanical properties.¹⁶ The main advantages of FEM are (1) simplicity of the experimental setup for excitation and detection, (2) excellent UHV conditions with the possibility of a range

of *in situ* treatments, (3) visualization of the apex motion in two directions, (4) access to high electric field (i.e., capacitive) tuning, (5) enhanced sensitivity to higher eigenmodes¹⁷ by image analysis, and finally (6) the FE current measurement has no loss of sensitivity for detecting vibrations as the size of the cantilever is reduced even down to single wall carbon nanotubes. The FE current (without detection) has been exploited in the detection of the resonances of top-down NEMS cantilevers.¹⁸ Looking further ahead one can imagine a new generation of time varying FE devices where the modulation is directly at the source. Recently, this configuration has been used to fabricate a “Nanotube Radio” where the resonating-nanotube-field emitter serves as the antenna, tuner, amplifier, and demodulator.¹⁹ A final example is the observation and modeling of auto-oscillations of nanowires without external ac driving in this configuration, opening the way for nanometric dc to ac conversion.²⁰

At present an in-depth study of the resonance behavior of the singly clamped configuration is now required to fully understand the influence of external perturbations for applications such as those mentioned above. For example, the large tensions generated by electric field induced mechanical stress that tune the resonance frequencies, as well as the complex boundary conditions at both the free and clamped nanowire ends, complicate the interpretation of the resonance frequencies necessary for extracting intrinsic mechanical parameters in the FE configuration. The approach here will be to develop analytical solutions as much as possible, which lead to more in-depth understanding and avoid time consuming and opaque numerical simulations.

In this paper, we both theoretically and experimentally explore the resonance behavior of singly clamped SiC nanowires on W tips over a large range of applied static voltages. We mostly address linear response in this paper. Complementary experiments have been realized both in the SEM and FEM. We have focused on the electrostatic tuning in the FEM for a correct determination of Young’s modulus, on the Q -factor measurements and on the boundary conditions for the nanowire’s movement. Parallel theoretical modeling is given, with validity intervals for the different static voltage ranges and for the influence of the boundary conditions. We have experimentally and theoretically investigated the influence of the electrostatic stress direction on the eigenfrequencies. An important result is that nanowire resonators glued on tungsten tips in a bottom-up spirit and heat treated can have higher quality factors than top-down fabricated nanoresonators of the same volume.

The paper is organized as follows: Section II briefly describes our experimental setup (for more details see Ref. 17 or 20). A theoretical analysis of our system is given in Sec. III, and Sec. IV is dedicated to the presentation and the interpretation of our results. A brief conclusion is given in Sec. V.

II. EXPERIMENTAL SETUP

The samples studied here were monocrystalline SiC nanowires covered by nanometer-thick turbostratic amorphous carbon layers (denoted as SiC@C; sometimes termed nano-

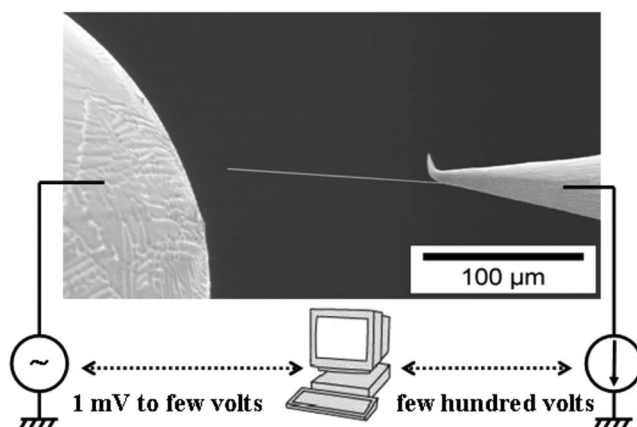


FIG. 1. Nanowire in SEM configuration. The position of the excitation anode with respect to the nanowire can be changed in all directions by steps down to 20 nm. Voltages V_{ac} and V_{dc} can be computer controlled.

cable). Details of the fabrication of the nanowires were given elsewhere.^{21,22}

In the SEM configuration, the tip with the nanowire is positioned on a X-Y nanomanipulator (Fig. 1) at a dc voltage V_{dc} with respect to the ground.¹⁴ An anode tip is placed in the vicinity of the nanowire on a Z nanomanipulator at an ac voltage V_{ac} with respect to the ground. Those two voltages polarize the tip and nanowire giving rise to electrical forces between the nanowire and the anode. Natural mechanical vibration modes of the singly clamped nanowire are excited when there is a frequency match with V_{ac} . The major advantages of this configuration are direct visualization of the oscillations, control of the geometry, and the possibility to excite and observe oscillations in zero field. This last is important because it gives the frequencies of the untuned natural modes necessary for confirmation of the modeling. As with FEM, we can also measure the resonance frequencies as a function of the applied dc voltage, but over the whole tuning range. Finally, the line mode of the SEM (where the scan is only made along one horizontal line instead of the whole screen) can be used for determination the amplitude of the oscillation, although this is difficult due to the slow time response (2 s/scan). The disadvantages of this configuration are the poorer vacuum, beam induced pollution which is particularly perturbing for high Q and small volume resonators, reduced sensitivity to the amplitude and the size of cantilever, and lack of *in situ* treatments.

In the FEM configuration, the tip with the nanowire is mounted on a heating loop inside an UHV chamber at 10^{-10} Torr (Fig. 2). The tip temperature is controlled by passing a current through the loop and it is measured by a micropyrometer. The loop is polarized with a dc voltage V_{dc} and electrons are field emitted from the nanowire’s apex where the electric field is enhanced by the tip effect. This FE current is amplified by a microchannel-plate (MCP) and creates fluorescence on a phosphor screen. Previous studies showed that heat treatment could raise the Q factor of top-down³ and bottom-up⁴ fabricated cantilevers by up to a factor of 100. Measurements are made at room temperature and after 5 min heating cycles of ever increasing tempera-

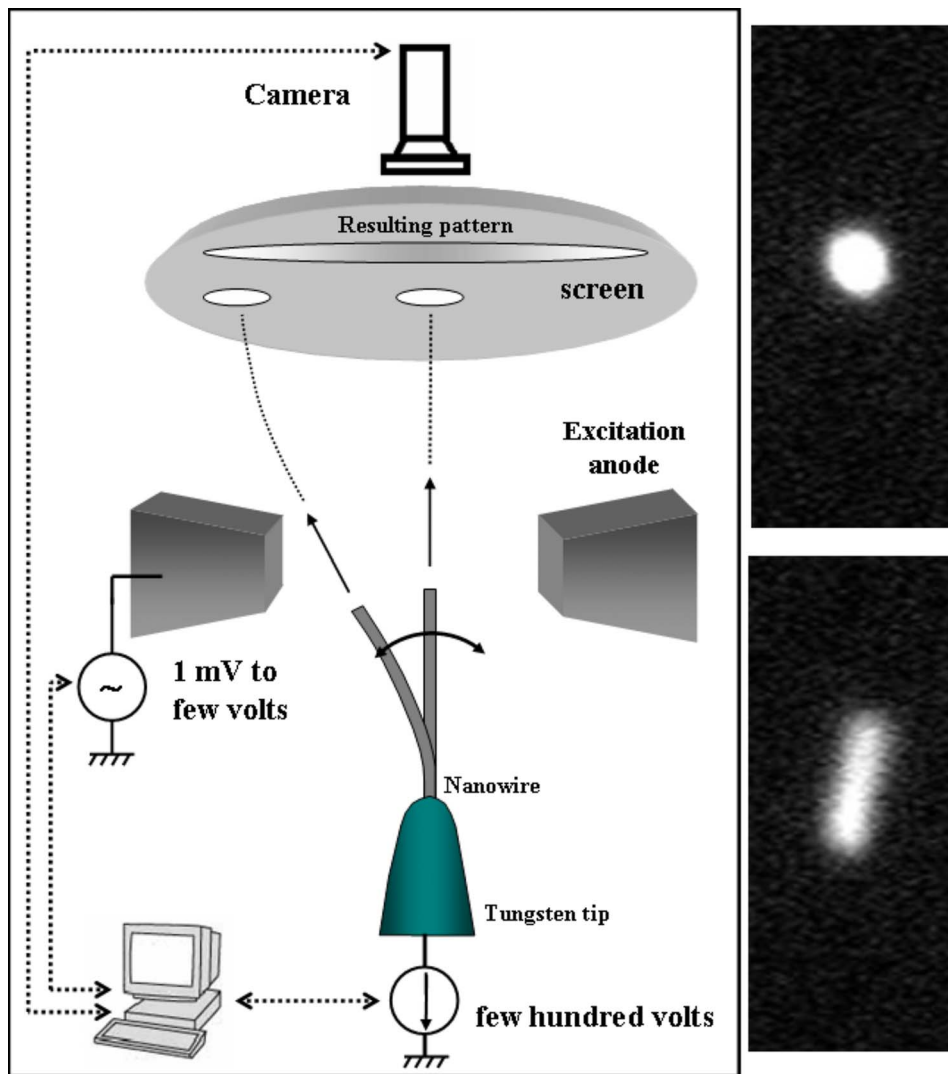


FIG. 2. (Color online) FE configuration (left) and SiC(3) apex FEM images (right) out of (up) and in (down) resonances. dc and ac voltages can be computer controlled. A LABVIEW® program acquires and analyzes in-line the camera image in order to extract the amplitude of the oscillation.

tures. These cycles progressively desorb surface adsorbates and perhaps anneal the contact and the nanowire defects. A more detailed study outside the scope of this paper must be carried out to determine the interplay between these different mechanisms. After a heating cycle, the nanowire's temperature cools down to room temperature in less than a minute²³ and then we have about 1 h before adsorbates recover the surface. Four excitation anodes are arranged as a quadrupole around the nanowire's tip and polarized with an ac voltage V_{ac} . The nanowires are excited by the same mechanism as in the SEM configuration and the resonances are detected by the widening of the FE pattern on the MCP.^{16,17}

The amplitude of the oscillations can be accurately and sensitively determined even during frequency scans from the image blurring.¹⁷ Our video camera functions at 25 Hz, giving only an averaged image of the oscillating emission pattern. A minimum dc tension typically of a few hundred volts is necessary to extract electrons and create the FE pattern. We studied six SiC nanowires in these experiments, denoted as SiC(1)-SiC(6). The density of SiC is $\rho=3200$ kg/m³ and the sizes of the nanowires are given in Table I.

III. THEORETICAL MODEL

We sketch here the physics of the motion of a singly clamped rod even though it is a textbook problem²⁴ because this forms a necessary base for our study. This model is completed with different elements concerning the free and the clamped boundary conditions. We compute expansions for the low and high applied voltage ranges with precise ranges of validity that are useful for interpreting experimental data.

TABLE I. Radii and lengths of our nanowires.

Nano wire	Radius (nm)	Length (μm)
SiC(1)	103	93
SiC(2)	143	128
SiC(3)	17.5	2.5
SiC(4)	135	243
SiC(5)	113	103
SiC(6)	104	32.5

The resonances are determined by nontrivial solutions of the equation of motion in the absence of external driving. We consider only a symmetric nanowire-anode geometry when at rest. This equation of motion can be easily expressed in the limit of low angles of the rod with respect to the equilibrium position,

$$\mu \frac{\partial^2 y}{\partial t^2} + \gamma \mu \frac{\partial y}{\partial t} = -YI \frac{\partial^4 y}{\partial x^4} + T \frac{\partial^2 y}{\partial x^2} + f(x, y), \quad (1)$$

where x is the position along the nanowire, $y(x, t)$ is the lateral displacement, ρ is the density, $\mu = \pi r^2 \rho$ is the mass per unit length, $I = \pi r^4 / 4$ is the “area moment of inertia,” Y is Young’s modulus, and γ is the damping coefficient. The axial stress T , due to electrostatic pulling, is assumed to be constant along the nanowire. $f(x, y)$ is the transversal electric force along the nanowire that exists when it is at a finite amplitude away from the symmetric equilibrium position. Electrostatic simulations of straight and tilted nanowires show that a large charge is induced by capacitance at the nanowire ends leading to a net pulling force T localized at the nanowire’s apex. The charge induced forces on the sides tend to cancel and the small net lateral force has a negligible effect on the mode frequencies compared to $T \partial^2 y / \partial x^2$.

Our Q factors are very high [$Q = \omega / \gamma > 1000$ and up to 160 000 (Ref. 4)] and thus damping can be neglected when looking for solutions $y(x, t) = y_0(x) e^{i\omega t}$ at the angular frequencies $\omega = 2\pi f$ (it can be reintroduced simply by changing ω^2 with $\omega^2 - i\gamma\omega$). We get

$$\frac{\partial^4 y_0}{\partial x^4} - \frac{\kappa^2}{L^2} \frac{\partial^2 y_0}{\partial x^2} - \frac{\omega^2 \kappa^2}{c^2 L^2} y_0 = 0, \quad (2)$$

with $\kappa^2 = TL^2 / (YI)$ and $c^2 = T / \mu$. The solution of this equation is

$$y_0 = A \cosh \frac{qx}{L} + B \sinh \frac{qx}{L} + C \cos \frac{kx}{L} + D \sin \frac{kx}{L}, \quad (3)$$

with k and q found from

$$q^2 = k^2 + \kappa^2, \quad (4)$$

$$\omega = \frac{cqk}{\kappa L}. \quad (5)$$

The constants A , B , C , and D can be calculated from the boundary and initial conditions. At the extremities of the nanowire, we assume no displacement and no slope for $x=0$ and no torque and force equilibrium for $x=L$,

$$(y_0)_{x=0} = 0, \quad (6)$$

$$\left(\frac{\partial y_0}{\partial x} \right)_{x=0} = 0, \quad (7)$$

$$\left(\frac{\partial^2 y_0}{\partial x^2} \right)_{x=L} = 0, \quad (8)$$

$$\left(-YI \frac{\partial^3 y_0}{\partial x^3} + \xi T \frac{\partial y_0}{\partial x} \right)_{x=L} = 0. \quad (9)$$

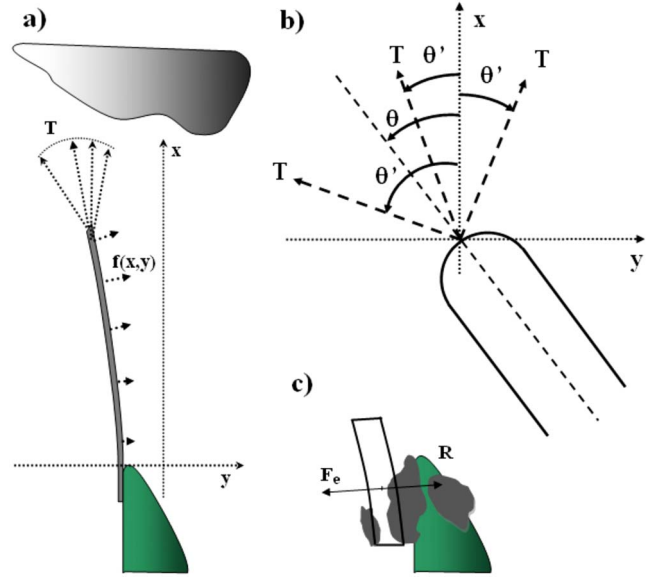


FIG. 3. (Color online) Boundary conditions on the nanowire: (a) External forces acting on the nanowire. The different possible orientations of \mathbf{T} correspond to different values of ξ . (b) A zoom on the nanowire’s apex. We have $\xi = \sin(\theta - \theta') / \sin \theta$. (c) Zoom on the nanowire’s clamped end. The elastic force \mathbf{R} in the glue is canceled by the restoring force in the nanowire \mathbf{F} [$F = (-YI \partial^3 y / \partial x^3 + \xi T \partial y / \partial x)_{x=0}$] (see Sec. IV).

The dimensionless constant ξ is a useful parameter that allows us to take into account the fact that the electrostatic force T may have a nonzero angle with the nanowire’s axis at the apex [see Figs. 3(a) and 3(b)]. If $\xi = 0$, then \mathbf{T} perfectly follows the direction of the apex axis; if $\xi = 1$, then \mathbf{T} is fixed along the direction of the straight nanowire axis. The exact value of ξ depends both on the shape of the apex and on the anode geometry (e.g., concavity of the anode) of the NEMS. Analog problems can be found in fluid mechanics, where the force acting on the end of a garden hose by reaction to the water jet is not perfectly oriented by the direction of the tube’s end.²⁵ Determining ξ theoretically demands the tedious resolution of Laplace’s equation in three dimensions for rods of varying tilts and bending. Instead, we have carried out an experimental investigation of the ξ parameter, which is presented at the beginning of the next section. Up to the first order in θ ($\tan \theta = \partial y / \partial x$), Eq. (1) is still correct.

The condition for existence of nontrivial solutions of Eq. (2) satisfying boundary conditions (6)–(9) is

$$(2q^2 k^2 + \xi \kappa^4) \cosh q \cos k + q^4 + k^4 - \xi \kappa^4 + (2\xi - 1) q k \kappa^2 \sinh q \sin k = 0. \quad (10)$$

Resonant frequencies are obtained by inserting values of k and q obtained from Eqs. (4) and (10) into Eq. (5). The electric force T due to capacitance forces can be expressed as a function of the electric field E at the surface of the nanowire,

$$\mathbf{T} = \int_{\text{wire surface}} \frac{\epsilon_0 E^2}{2} \mathbf{n} dS, \quad (11)$$

with \mathbf{n} as the unit vector of the surface element dS and ϵ_0 as the vacuum dielectric permittivity. The electric field E is proportional to the applied voltage V_A and thus $T \propto V_A^2$. From electrostatics $E = \beta V_A$, with β as a constant, the geometrical amplification factor. β is determined both by the environment, for example, through the distance between the nanowire and the anode, and by the nanowire itself through its geometry (it scales roughly with the nanowire aspect ratio L/r). Since the electric field is very much enhanced at the nanowire's apex and forces on the sides do not play in the tuning tension, the integral in Eq. (11) can be taken only on the surface at the end of the nanowire, which allows us to estimate $T \simeq \epsilon_0 \pi r^2 E_{max}^2 / 2 = \epsilon_0 \pi r^2 \beta_{max}^2 V_A^2 / 2$. A numerical value is immediately found because FE occurs when the maximum field satisfies $7 > E_{max} > 3$ V/nm.

For convenience, we define V_C to be the voltage giving $T = YI/L^2$ ($\kappa^2 = 1$). Later in this section, we show that V_C allows us to define regions of low and high voltage behavior. We have

$$T = \frac{YI V_A^2}{L^2 V_C^2}. \quad (12)$$

When the geometry is changed, for example, if the nanowire is placed further from the anode, it is enough to correct the value of β (and thus V_C) to obtain the new behavior of the nanowire. In our geometry T is always positive because we only have stress in our nanowire and never slack. This means that supplementary eigenmodes described by Üstünel *et al.*¹¹ do not exist.

The dependence of the first three eigenfrequencies on the V_A for different values of ξ is given in Fig. 4. We show in Sec. IV that experiments give $\xi \simeq 1$, so we will use $\xi = 1$ until the end of this section. The figure shows one curious and counterintuitive phenomenon for the more commonly used boundary condition of $\xi = 0.0$, which is that the first mode decreases in frequency as the tension is increased (see explanation caption in Fig. 4). We have not found an experimental confirmation of this phenomenon in the literature and in principle it leads to a confusion in the identification of the modes in FE experiments where $T = 0$ is not accessible and thus in the determination of Young's modulus.

One can distinguish in Fig. 4 three distinct ranges: low, intermediate, and high (linear). Most of our experiments are situated in the first range with low electrostatic pulling. Sazonova²⁶ already pointed out that in this low voltage range,

$$\omega^2 - \omega(0)^2 \propto V_A^2, \quad (13)$$

with $\omega(0)$ the corresponding eigenfrequency for $V_A = 0$.

To intuitively understand the effect of T on the eigenfrequencies to first order, we can consider each eigenmode of our nanowire as a harmonic oscillator with 1 degree of freedom. The theory of the harmonic oscillator tells us that " $\omega^2 = \text{return force per unit displacement and per unit mass}$,"²⁷ and since we have an elastic return force that gives $\omega(0)$ and an electrical perturbation force proportional to V_A^2 , we get Eq. (13).

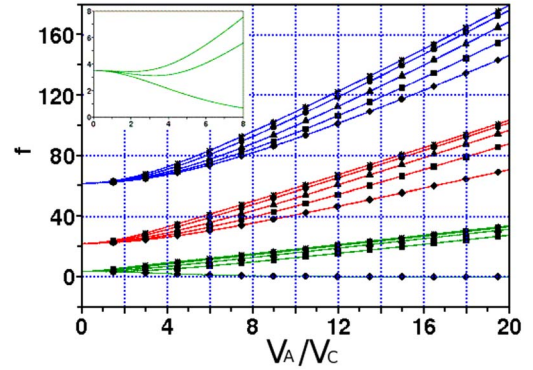


FIG. 4. (Color online) Simulation of the resonant frequencies of the first three eigenmodes as a function of V_A in the FEM for $\xi = 0$ (\blacklozenge), $\xi = 0.2$ (\blacksquare), $\xi = 0.5$ (\blacktriangle), $\xi = 1$ (\bullet), and $\xi = 1.5$ ($*$). The voltage is normalized to V_C [Eq. (12)] and the frequencies f_n are normalized to $\sqrt{YI/\mu L^4}/2\pi$. In the low voltage zone, with $\xi = 1$ ($V_A < 1.8V_C$ for the first mode), there is a linear dependence for $\omega^2(V_A^2)$ with $(\omega_0)^2$ the free coefficient [Eq. (14)] and in the high voltage zone ($V_A > 10V_C$ for the first mode), there is a linear dependence $\omega(V_A)$ with $-V_C$ the root [Eq. (18)]. In the intermediate zone, both elastic and electrostatic contributions to ω^2 are important, which means that the exact solution of Eqs. (4), (5), and (10) must be used. The inset is a low voltage zoom for the first eigenmode with $\xi = 0$, $\xi = 0.05$, and $\xi = 0.1$. One can see that when ξ is precisely zero (electrostatic stress completely oriented along the end axis), the frequency of the first mode converges to zero as $V_A \rightarrow \infty$. This is because when at infinite tension the shape of the nanowire out of equilibrium is a straight line, and thus, there is no return force. As well the shapes and frequencies of the superior modes become identical with the doubly clamped configuration with the same T . For low values of ξ , the first mode has a minimum eigenfrequency for a nonzero voltage.

Sapmaz *et al.*¹⁰ already calculated the expansion for a doubly clamped rod up to the first order in T (and thus V_A^2). We have focused on the singly clamped configuration, where the "free end" boundary conditions (8) and (9) significantly change the resonance behavior of the rod. To check the validity interval of Eq. (13), we computed the Taylor expansion of ω^2 in V_A^2 from Eqs. (4), (5), and (10),

$$\omega_n^2 = \omega_n(0)^2 \left(1 + X_n \frac{V_A^2}{V_C^2} + Y_n \frac{V_A^4}{V_C^4} + \dots \right), \quad (14)$$

where $n \in \mathbb{N}$ is the mode's index, β_n is the solution of $\cos \beta_n \cosh \beta_n = -1$ inside the interval $[n\pi, (n+1)\pi]$, and

$$\omega_n(0)^2 = \frac{YI\beta_n^4}{\mu L^4}, \quad (15)$$

$$X_n = \frac{2 \sinh \beta_n + \beta_n [\cosh \beta_n - (-1)^n]}{\beta_n^3 [\cosh \beta_n + (-1)^n]}, \quad (16)$$

$$Y_n = \frac{4\beta_n[\cosh^2 \beta_n + 1] - \tanh \beta_n[(\beta_n^2 - 1)\cosh^2 \beta_n + 1] + (-1)^n[8\beta_n \cosh \beta_n + \sinh^3 \beta_n - \beta_n^2 \sinh \beta_n] - \beta_n^3 \sinh^2 \beta_n}{2(-1)^{n+1}\beta_n^6 \tanh \beta_n[\cosh \beta_n + (-1)^n]^3}. \quad (17)$$

We have shown that these formulas match numerical solutions of Eqs. (4), (5), and (10). For the first mode ($n=0$), $\beta_0 \approx 1.875$, $X_0 \approx 0.376$, and $Y_0 \approx -0.01$. This means that limiting the expansion of ω^2 in V_A^2/V_C^2 to first order is a good approximation (within 3% of error) for $\omega(V_A) < 1.5\omega(0)$ ($V_A < 1.8V_C$). Our experiments were usually in this range of frequency.

For higher modes (higher n and β_n), $|X_n| \sim 1/\beta_n^2$, and $|Y_n| \sim 1/\beta_n^6$, diminishing the relative contribution of the higher order terms with respect to the first order term. This means that for our experiments, usually situated in the low voltage regime, we have a linear dependence of ω^2 on V_A^2 , with $\omega(0)^2$ the free term, which allows simple experimental determination of Young’s modulus even in the FEM, where $\omega(0)^2$ is not directly accessible.

In the high voltage limit ($V_A \gg V_C$), we have a quasilinear variation of the eigenfrequencies with V_A ,

$$\omega_n = \frac{2n+1}{2L^2} \sqrt{\frac{YI}{\mu} \left[\frac{V_A}{V_C} + 1 + \frac{4+(2n+1)^2\pi^2 V_C}{8 V_A} + \dots \right]}, \quad (18)$$

where $n \in \mathbb{N}$ and the first two terms were given in Ref. 16. This range is not easy to experimentally obtain; one needs $V_A > 10V_C$ in order to have the linear dependence at better than 1.5% for the first mode, and this limit rises with the mode index. Experimental determination of Young’s modulus can only be made by using the free term of the linear interpolation, as V_C is unknown. Since extrapolation is made quite far from the data (we want to determine ω for $V_A=0$ by using ω for $V_A \gg V_C$), it is useful to include additional terms

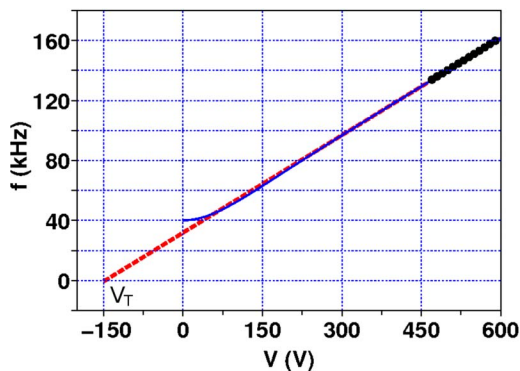


FIG. 5. (Color online) Example of experimental frequency-voltage dependence (●) with exact theoretical interpolation (----) giving $V_C=80$ V. The dotted line (—) is a linear interpolation giving $V_T=-147$ V. Although data seem to fall on a straight line, we are not yet in the linear range given by the first two terms of expansion 18 since $V_T \neq -V_C$. We can see that $|V_T|$ is still bigger than one-tenth of the experimental voltage.

from Eq. (18). Interpolation with Eq. (18) on simulated data with Eqs. (4), (5), and (10) between $V_A=8V_C$ and $V_A=10V_C$ yielded Young’s modulus with 10% of error.

Field emission experiments are usually over a relatively small voltage range compared to the full characteristic $\omega_n(V_A)$ curves [solutions of the Eqs. (4), (5), and (10)]. This means that experimental $\omega_n(V_A)$ curves at first glance usually look like straight lines, even if we are not in the high voltage range where expansion (18) can be stopped at the linear and constant terms (see Fig. 5). This is enhanced because the opposing signs in different terms of the expansions cause $\omega(V_A)$ to appear to be linear even though it converges extremely slowly to the solution $\omega(V_A)$ as $V_A \rightarrow \infty$ (observe Fig. 5 closely). An easy way to check in which range we are is to use linear interpolation for the experimental data. Let V_T be the zero crossing of this linear interpolation (note $V_T < 0$). If the experiment is really in the linear range (e.g., $V_A/V_C > 10$), then from Eq. (18) $V_T = -V_C$. If V_A is smaller than $10V_C$, then the ratio of this applied voltage to $|V_T|$ is clearly smaller than 10, since $|V_T| > V_C$, as it can be seen in Fig. 4 if we draw a tangent to the $\omega(V_A)$ curves. To summarize, one is in the high voltage linear range if and only if $V_A/|V_T| \geq 10$ for the first mode. In retrospect, the measurements of Ref. 16 were probably not in the linear range.

For a given mode, the slopes of the $\omega(V_A)$ curves are fixed by the value of V_C , with small slopes for high V_C and vice versa. To calculate V_C , one must calculate the geometrical factor β , which is usually difficult because one must resolve Laplace’s equation in the specific geometry. (It also varies during the oscillation but this is quadratic due to symmetry and we assume small oscillations.) However, it is clear that V_C increases with r and the distance to the anode and decreases with L . We have large slopes, and thus high NEMS frequency tunability, for long thin nanowires situated close to the anode. Experimental data for the slopes of the first mode range from 10 to 10^5 Hz/V (see Fig. 9 and Ref. 28).

The analysis can be pushed further to determine V_C (and thus β) from the experimental data. For example, V_A/V_C is directly related to the ratios of the different eigenfrequencies. These ratios taken from Fig. 4 are shown in Fig. 6. The curves are universal for singly clamped rods of any uniform cross section, satisfying boundary conditions (6)–(9) with $\xi = 1$. Mode ratios can also be checked to experimentally verify the $2n+1$ ratios in the high voltage regime, although we need even higher V_A than for the first mode. As an aside this provides an independent measure of β that could in turn be used to extract the work function ϕ of the nanowire apex from the slope of the Fowler–Nordheim plot, which gives only $\phi^{3/2}/\beta$.

IV. RESULTS AND DISCUSSION

In this section, we show an extensive body of experimental measurements of the resonance frequencies of different

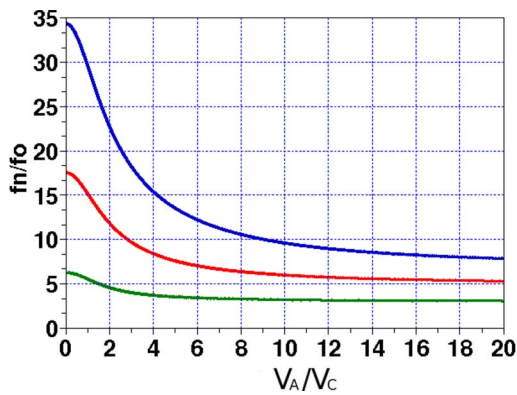


FIG. 6. (Color online) Ratios of the second (bottom curve), third (middle curve), and fourth (upper curve) mode eigenfrequencies to the first mode eigenfrequency as a function of V_A normalized to V_C . These curves are universal for prism shaped homogenous singly clamped cantilevers satisfying boundary conditions (6)–(9) with $\xi = 1$. The values for zero voltage are 6.27, 17.55, and 34.39.

nanowires versus applied voltage and compare these results to the theoretical model. The good agreement allows us to determine Young's modulus even in the FEM. Furthermore, we study the Q factor as a function of heat treatment.

First, we present an experimental investigation of the “force equilibrium” boundary condition [Eq. (9)]. The value of ξ should be influenced by the environment: a concave extraction anode should decrease ξ and a convex one should increase it. We made two f - V measurements on the first mode of SiC(5) and we fit them with theoretical predictions (Fig. 4) in order to extract the value of ξ (together with Y and V_C). Experimental data (Fig. 7) is coherent with $\xi=0.81$ for the concave configuration and $\xi=1.2$ for the convex configuration (Fig. 8). This means that the direction of the electrostatic stress T has only a small variation during the oscillation

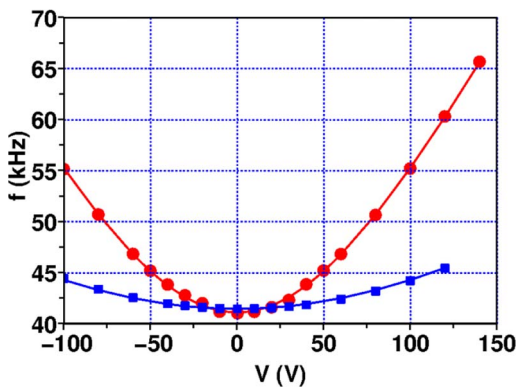


FIG. 7. (Color online) Experimental data on SiC(5) for concave (■) and convex (●) extraction anode configurations and fits to theory (solid lines). The V_C value for the convex configuration is inferior (and thus β is larger) to that of the concave one, making the resonance more sensitive to V_A . In the convex configuration, the general formulas (4), (5), and (10) have to be used for interpolation since $V_A > 2V_C$. Interpolated values of ξ are close to 1.0 in both cases (0.81, concave and 1.2, convex), which means that the direction of the electrostatic stress is not much influenced by the shape of the wall or by the position of the nanowire during the oscillation.

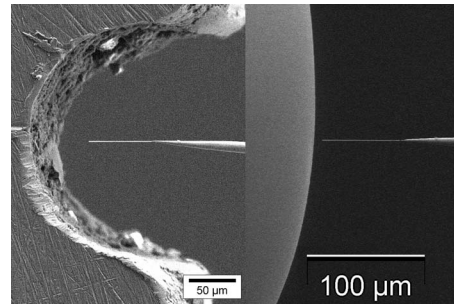


FIG. 8. SiC(5) in front of a concave (left) and convex (right) wall. We placed the nanowire further from the concave wall to compensate for the curvature radius which was bigger for the convex wall.

($\xi \approx 1$) and this variation depends on the concavity of the anode in front of the nanowire. The low dependence of the eigenfrequencies on ξ for this range of values (Fig. 4) and the rather close values of ξ measured for these extreme configurations means that the use of $\xi=1$ in the previous section was a good approximation. As well, the $\xi > 0.1$ means that we will not observe a decrease in the frequency of the first mode ($n=0$, see inset Fig. 4) and resolves the problem of identifying the modes in FEM.

Young's modulus can be determined from the measured eigenfrequencies. Experiments usually lie in the low voltage range, where Eq. (14) can be used. In the SEM, the measurement of the zero voltage eigenfrequency is direct compared to FEM where it has to be extrapolated from the linear $\omega^2(V_A^2)$ dependence (in FE, we always have $V_A < 0$ in order to emit electrons).

Our results are presented in Table II, showing a large scatter in the measured values for the SiC Young's modulus. Those values are nevertheless compatible with results found in the literature, differences being attributed to various allotropic states of SiC and to different orientations of the eigenmodes with respect to the crystalline planes.^{29–35} These Young's moduli confirm the high resolution TEM observations, which indicate that small and large size nanowires have a better crystalline structure than the average size ones.

We have found that the dependence of the mode resonances on V_A for each nanowire fits more or less well the simplest application of the theory presented above, and that the data must be examined in detail in order to come to a full understanding. For each nanowire, the ratios between the zero voltage eigenfrequencies of different modes give us an idea of the deviation of the nanowire from perfection and hence in the error of the experimental Young's modulus. Comparison of the values in Table II to Fig. 6 shows a correct ratio for SiC(2) and SiC(6), lower ratios for SiC(4) and SiC(5), and higher ratios for SiC(1). SiC(3) was measured only in its first mode.

SiC(2) was only studied in the FEM. The dependence of the first two eigenfrequencies on V_A is presented in Fig. 9. We attribute the slight difference between the experimental determination of the ratio of the frequencies of the first two modes at zero voltage by extrapolation using Eq. (14) and its theoretical prediction to small geometrical defects (for example, small variations of the radius along the nanowire).

TABLE II. Young's moduli as extracted from the experimental FE and SEM data. The two methods give very similar values (see Fig. 1 below). Frequencies correspond to the free (zero voltage) eigenmodes. SiC(4), SiC(5), and SiC(6) were studied in SEM configuration, SiC(2) and SiC(3) were studied in FEM configuration, and SiC(1) was studied in both configurations.

Nano wire	Mode	Frequency (kHz)	Young modulus (GPa)
SiC(1)	1	28.44	230
SiC(1)	2	213.47	330
SiC(1)	3	642.36	380
SiC(2)	1	22.36	268
SiC(2)	2	144.43	285
SiC(3)	1	11150	660
SiC(4)	1	7.76	
SiC(4)	2	42.91	534 ^a
SiC(4)	3	115.73	
SiC(5)	1	41.05	750 ^a
SiC(5)	2	216.39	
SiC(6)	1	318.95	429
SiC(6)	2	2007.0	432.5

^aWith elastic contact correction (see text).

This small 3% difference yields a 6% difference in Young's modulus (see Table II). SiC(6) was only studied in the SEM configuration and yielded the correct ratio of the first two eigenfrequencies (<0.5% difference with respect to the theory) and Young's modulus (see Table II) in the average range of our nanowires and of the values found in literature. SiC(4) was also only studied in the SEM configuration. It showed ratios of first to second mode frequencies of 5.53 instead of the theoretical of 6.27 and first to third mode frequencies of 14.91 instead of the theoretical of 17.55 (Fig. 6). We propose that this nanowire was not perfectly attached to the tip and the glue coupling showed some elastic response. Such a coupling has been modeled in a detailed way.³⁶ We present here a simpler model, with 1 additional degree of freedom that can explain the observed behavior.

The glued part of the nanowire is much shorter than the nanowire itself, which implies that the "no displacement" boundary condition (6) is well respected even with a glue having some elasticity. However, the tilt of the nanowire at the tip contact [boundary condition (7)] is no longer negligible and is to a first approximation the ratio between the (very small) nanowire displacement in the glued part and the (very small) length of this glued part. This displacement gives rise to an elastic force [Fig. 3(c)] that must be canceled by the elasticity inside the nanowire,

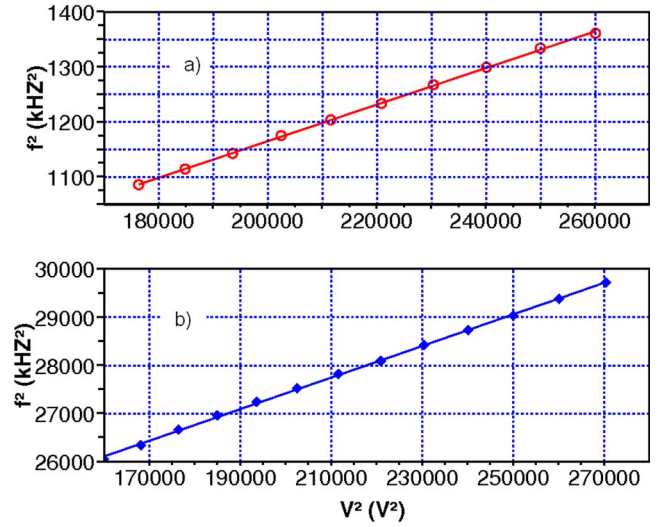


FIG. 9. (Color online) (a) First and (b) second mode frequencies as a function of applied voltage for SiC(2) measured in FEM. A linear dependence of f^2 versus V_A^2 is observed, as predicted by Eq. (14). The free coefficient of the regression yields the zero voltage eigenfrequency and thus Young's modulus.

$$\left(\frac{\partial y_0}{\partial x}\right)_{x=0} \propto \left(T\frac{\partial y_0}{\partial x} - YI\frac{\partial^3 y_0}{\partial x^3}\right)_{x=0}. \quad (19)$$

We can rewrite Eq. (19) with a dimensionless constant α ,

$$\left(\frac{\partial y_0}{\partial x} + \alpha L^2\frac{\partial^3 y_0}{\partial x^3} - \alpha\kappa^2\frac{\partial y_0}{\partial x}\right)_{x=0} = 0. \quad (20)$$

Our measured eigenfrequencies for the first three modes of SiC(4) are now very well described (better than 0.5%) with the two free parameters, giving $Y=534$ GPa and $\alpha=0.0235$. The small value of α confirms that the elastic glue is a small correction to the nanowire's oscillation.

This shows that one must be very careful in order to extract accurate values of Young's modulus from the eigenfrequencies. If we neglect the α correction for SiC(4), Young's modulus as inferred from the first three eigenmodes would

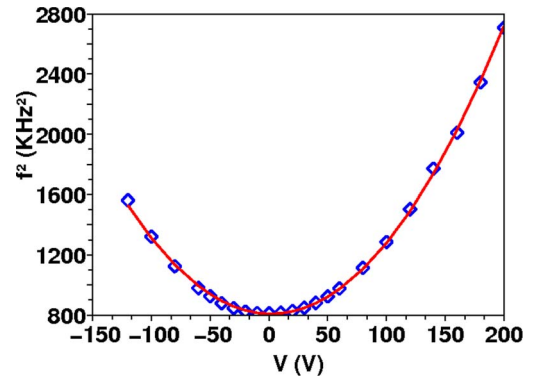


FIG. 10. (Color online) Square of the eigenfrequency of the first mode as a function of V_A (\diamond) in the SEM. Fit with Eq. (14) (—) up to the V_A^2 term describes well our data with an asymmetry of 1.8 V. Y and V_C are extracted from the fit parameters.

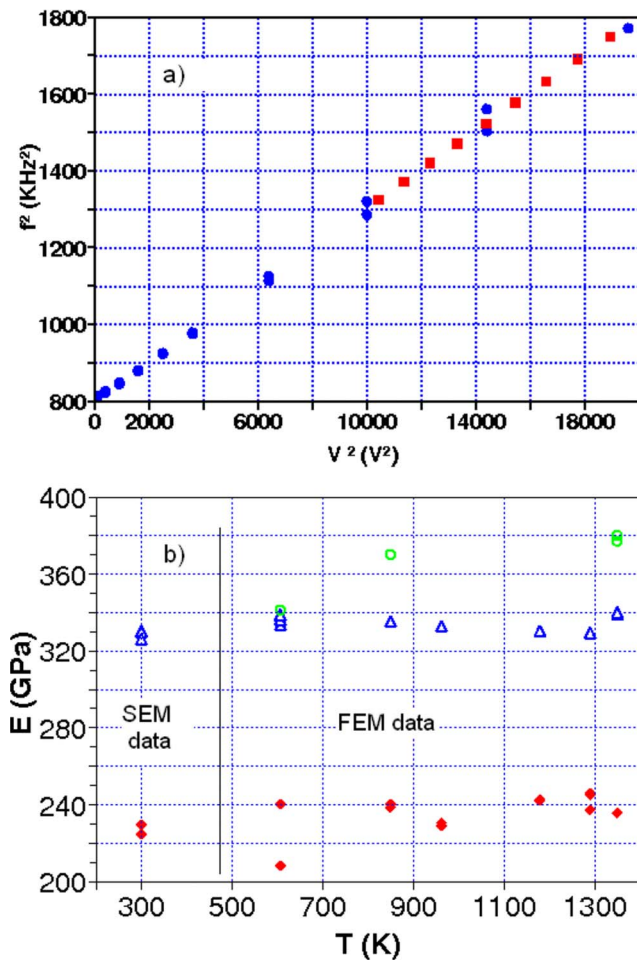


FIG. 11. (Color online) (a) $f^2(V_A^2)$ curve for SiC(1) in the SEM (●) and FEM (■) for the first eigenmode. The SEM measurements were made for both positive and negative voltages. The extracted V_C values are, respectively, 77.82 V (SEM) and 175.59 V (FEM). For this plot, the voltages of the FE data were normalized to have the same V_C as for the SEM configuration. With this condition, no measurable difference can be found between the two curves, as it can also be seen in graph (b): Young's modulus as extracted from the first (◆), second (△), and third (○) modes as a function of the prior heating. Ambient temperature values (300 K) correspond to the SEM measurements, the rest of the points were extracted from FE data. No measurable difference can be seen between the two configurations for a given eigenmode. The differences in Young's moduli extracted from the different modes is consistent with the inferred ratio of the zero voltage eigenfrequencies and we attribute them to geometrical defects.

be respectively 471, 366, and 340 GPa. Observation of at least two eigenmodes with a correct ratio for the eigenfrequencies or an α correction is necessary for a reliable result.

SiC(5) showed in the SEM configuration the same kind of behavior, with a ratio of the first two eigenfrequencies of 5.3. Application of the same model as for SiC(4) yielded a high Young's modulus ($Y=750$ GPa) and $\alpha=0.042$. This matches the highest value we have found in the literature for a bulk single crystal of 748 GPa.³³

The voltage dependence of the first eigenfrequency of SiC(3) was only measured in FEM. Experimental data gives

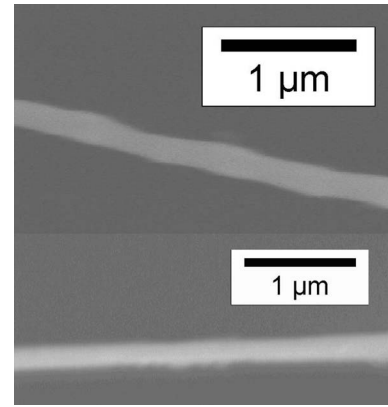


FIG. 12. SEM image of SiC(1) (upper image) and SiC(6) (lower). SiC(1) shows variations of the radius, which cause departure from the singly clamped beam theory. The absence of defects on SiC(6) gives good agreement between theory and experiment.

a V_C value of 313 V. Since our measurements were made in the range of 260–320 V, we are still in the low voltage range [Eq. (14)]. The minimum measurable amplitude was around 5 nm for $L=2.5$ μm , making our FE imaging technique an alternative to capacitive,^{38,39} magnetomotive,^{40,41} or optical^{3,42,43} detection of small displacements.

We have also made comparative measurements of Young's modulus for SiC(1) in the SEM and FEM. A wide range of positive and negative voltages were explored in the SEM, as represented in Fig. 10. Although we have a quadratic dependence of f^2 in V_A , as predicted by Eq. (14) for the low voltage range, we observe a shift of the minimum by 1.8 V. We attribute this voltage to the difference of work functions between the SiC and the tungsten of the excitation anode, but further study must be made to precisely determine this value.

We have good agreement between our two techniques for Young's modulus measurements (SEM and FEM), as can be seen in Fig. 11. Furthermore, no significant change in Young's modulus was found even after heating cycles to 1050 $^\circ\text{C}$, even when we had a drop in the Q factor by a factor of 30 (see below).

For SiC(1), the ratios of the superior mode eigenfrequencies at zero voltage with respect to the first mode eigenfrequency are higher than predicted by Eq. (14) (Fig. 6). This difference is present in both SEM and extrapolated FE values and is probably due to geometrical defects, more present in SiC(1) than in SiC(6), as we can see in Fig. 12. An elastic glue cannot explain ratios higher than predicted, as it can for the lower ratios of SiC(4) or SiC(5). In principle, such geometrical defects could also explain the behavior of SiC(4) or SiC(5), but the elastic glue model gives a very accurate description of the observed eigenfrequencies with only one extra parameter. This larger value of the eigenfrequencies ratios gives different values for SiC Young's modulus when they are extracted from the different mode measurements, as it can be seen in Fig. 11 or Table II. All those values are still compatible with the literature.

Measurements of the mechanical Q factor are complicated by the extreme sensitivity of our nanowires to external perturbation, which rapidly induces nonlinear mechanical re-

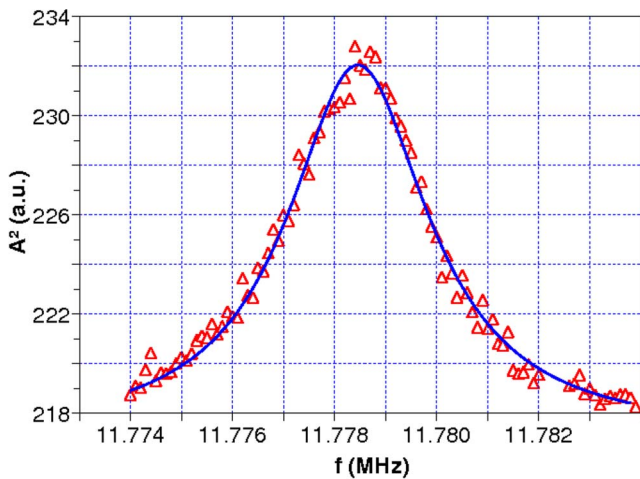


FIG. 13. (Color online) Response curve for SiC(3) in FEM and Lorentzian interpolation giving a Q factor of 3500.

sponses as the amplitude is increased. For reliable Q -factor measurements, linear Lorentzian response is necessary, and therefore we had to decrease our excitation to the minimum detectable amplitudes.

We have studied for SiC(1) the dependence of the Q factor on the heat treatment prior to measurement in FEM. The Q factor is measured by the response curve for a frequency scan through the resonance. An example of such a scan is given in Fig. 13 for SiC(3). Values of the SiC(1) Q factor after each heating cycle are given in Fig. 14. Damping is diminished by more than a factor of 100 after a heating at 1280 K compared to no heating. Three mechanisms can be proposed: removal of surface pollution, recrystallization of internal defects, or hardening of the contact glue. A value of the Q factor as high as 160 000 was achieved.⁴ We think that heating at 1320 K changed the properties of SiC itself, since the quality factor dropped by a factor of 30. Intensive heating can significantly change the shape of the nanowire creating dissipation zones, but these temperatures do not yet alter Young’s modulus.

The SiC(4) Q factor was measured in the SEM without prior heating, giving a value of about of 5000, in agreement with the value for SiC(1) at the lowest heating in the FEM

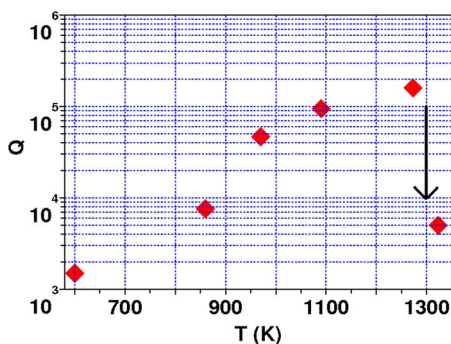


FIG. 14. (Color online) Quality factor at room temperature of SiC(1) as a function of the heat cleaning temperature. Measurements without any prior heating treatment were not possible because of the instability of the field emission.

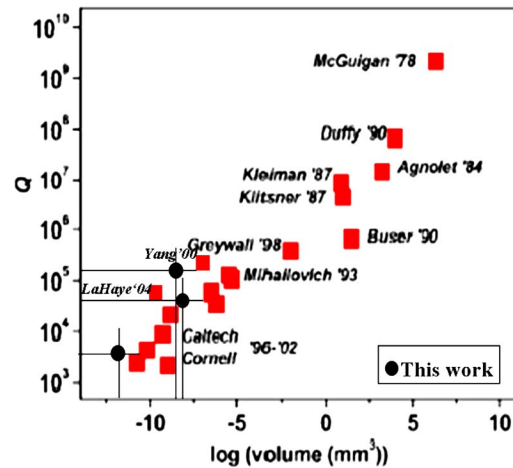


FIG. 15. (Color online) Q factor of resonators as a function of their volume in log-log plot (Ref. 5), with recent results from (Ref. 3). Experimental data “LaHaye’ 04” was corrected with the value taken from the original paper (Ref. 38). Our room temperature values, 160 000 for SiC(1), 36 000 for SiC(2), and 3500 for SiC(3), are on or above the straight line that best describes the dependence of $\log Q$ as a function of $\log(\text{volume})$. Some measurements of other authors used in this diagram were made at low temperature (including LaHaye), which increases the Q factor (Ref. 37).

(300 °C). Measurements in the SEM were perturbed by the interaction of the nanowire with the SEM’s beam when in line mode.

Q -factor measurements in FEM were also made on SiC(2) and SiC(3). The values we found after heat treatment at about 1000 K were, respectively, 36 000 for SiC(2) and 3500 for SiC(3). Previous experimental studies show that the logarithm of the Q factor linearly increases with the logarithm of the resonator volume,⁵ as shown in Fig. 15. This supports the argument that damping is mainly on the surface, because the energy is stored in the volume and small objects have a bigger surface to volume ratio and thus lower Q factors. Figure 15 also shows that our bottom-up nanowires have greater Q factors than top-down fabricated resonators of the same volume.

V. SUMMARY AND CONCLUSION

We have theoretically studied the mechanical resonances of singly clamped rods subjected to strong electrical axial pulling forces that are attainable only at the nanoscale and that are of interest for NEMS. Simple expressions for the dependence of the resonance frequencies on the applied voltage in the low stress and high stress limits were computed. Validity ranges for those approximations were also presented. As well new boundary conditions were introduced in the theory for nonaxial forces at the open end and for elasticity in the contact fixation. These boundary conditions allow us to explain additional aspects of the resonance phenomenon, for example, they explain the absence in experiment of the predicted decrease in eigenfrequency of the first mode by the simplest theory.

Corresponding experimental studies were made of the resonances of different SiC nanowires in the FE and SEM

configurations and these measurements were analyzed with the developed theory. The nanowires studied were shown to mostly be in the low tension regime contrary to our previous assumptions. The $\omega(V_A)$ curves gave excellent agreement between theory and experiment as well as between the two experimental configurations of SEM and FEM.

The technique can be used in any voltage range if we replace the simple dependence in Eq. (14) with the more complicated solution of the Eqs. (4), (5), and (10). Comparison to SEM measurements shows no measurable difference between the two techniques (Fig. 11). Influence of the boundary conditions on the nanowire's movement and more specifically on the extracted Young's modulus value were discussed.

We have showed that *in situ* heat cleaning can multiply the Q factor of a nanowire by 100, which allowed our "bottom-up" fabricated SiC nanowires to reach the highest measured Q factor range for a given volume. Excessive heating can strongly affect the Q factor of a SiC nanowire without inducing a measurable difference in Young's modulus,

indicating that changes occur in a rather small volume such as the glue that attaches the nanowire to the tip or the nanowire's external atomic layers.

In conclusion, this theoretical structure now allows one to use FEM detection of mechanical resonances, which have many advantages, as an alternative technique to the SEM or TEM for measuring Young's modulus of individual nanowires and nanotubes. These measurements show that each individual nanowire has its own Young's modulus, Q factor, and contact fixation even when they come from the same batch and are nominally mounted by the same technique. As well these parameters can be tuned over a wide range by applying in-situ treatments.

ACKNOWLEDGMENTS

This research has been carried out within the Lyon Nanotube and Nanowire Working Group. M.C. thanks the Lebanese CNRS for financial support.

*pascal.vincent@lpmcn.univ-lyon1.fr

¹Z. Chen, J. Appenzeller, Y. M. Lin, J. Sippel-Oakley, A. G. Rinzler, J. Tang, S. J. Wind, P. M. Solomon, and P. Avouris, *Science* **311**, 1735 (2006).

²D. F. Mcguigan, C. C. Lam, R. Q. Gram, A. W. Hoffman, D. H. Douglass, and H. W. Gutche, *J. Low Temp. Phys.* **30**, 621 (1978).

³J. Yang, T. Ono, and M. Esashi, *Appl. Phys. Lett.* **77**, 3860 (2000).

⁴S. Perisanu, P. Vincent, A. Ayari, M. Choueib, M. Bechelany, D. Cornu, and S. T. Purcell, *Appl. Phys. Lett.* **90**, 043113 (2007).

⁵K. L. Ekinci and M. L. Roukes, *Rev. Sci. Instrum.* **76**, 061101 (2005).

⁶V. Sazonova, Y. Yaish, H. Üstünel, D. Roundy, T. A. Arias, and P. L. McEuen, *Nature (London)* **431**, 284 (2004).

⁷H. B. Peng, C. W. Chang, S. Aloni, T. D. Yuzvinsky, and A. Zettl, *Phys. Rev. Lett.* **97**, 087203 (2006).

⁸D. Garcia-Sanchez, A. San Paulo, M. J. Esplandiu, F. Perez-Murano, L. Forró, A. Aguasca, and A. Bachtold, *Phys. Rev. Lett.* **99**, 085501 (2007).

⁹B. Witkamp, M. Poot, and H. S. J. van der Zant, *Nano Lett.* **6**, 12, 2904 (2006).

¹⁰S. Sapmaz, Ya. M. Blanter, L. Gurevich, and H. S. J. van der Zant, *Phys. Rev. B* **67**, 235414 (2003).

¹¹H. Üstünel, D. Roundy, and T. A. Arias, *Nano Lett.* **5**, 523 (2005).

¹²P. Poncharal, Z. L. Wang, D. Ugarte, and W. A. de Heer, *Science* **283**, 1513 (1999).

¹³Z. L. Wang, R. P. Gao, P. Poncharal, W. A. de Heer, Z. R. Dai, and Z. W. Pan, *Mater. Sci. Eng., C* **16**, 3 (2001).

¹⁴M. F. Yu, G. J. Wagner, R. S. Ruoff, and M. J. Dyer, *Phys. Rev. B* **66**, 073406 (2002).

¹⁵S. Axelsson, E. E. B. Campbell, L. M. Jonsson, J. Kinaret, S. W. Lee, Y. W. Park, and M. Sveningsson, *New J. Phys.* **7**, 245 (2005).

¹⁶S. T. Purcell, P. Vincent, C. Journet, and V. T. Binh, *Phys. Rev. Lett.* **89**, 276103 (2002).

¹⁷S. Perisanu, P. Vincent, A. Ayari, M. Choueib, D. Guillot, M. Bechelany, D. Cornu, P. Miele, and S. T. Purcell, *Phys. Status Solidi A* **204**, 1645 (2007).

¹⁸D. V. Scheible, C. Weiss, J. P. Kotthaus, and R. H. Blick, *Phys. Rev. Lett.* **93**, 186801 (2004).

¹⁹K. Jensen, J. Weldon, H. Garcia, and A. Zettl, *Nano Lett.* **7**, 3508 (2007).

²⁰A. Ayari, P. Vincent, S. Perisanu, M. Choueib, V. Gouttenoire, M. Bechelany, D. Cornu, and S. T. Purcell, *Nano Lett.* **7**, 225 (2007).

²¹M. Bechelany, D. Cornu, and P. Miele, Patent Application No. WO 2006/067308 (pending).

²²M. Bechelany, D. Cornu, F. Chassagneux, S. Bernard, and P. Miele, *J. Optoelectron. Adv. Mater.* **8**, 638 (2006).

²³S. T. Purcell, P. Vincent, C. Journet, and V. Thien Binh, *Phys. Rev. Lett.* **88**, 105502 (2002).

²⁴See, for example, F. S. Tse, I. E. Morse, and R. T. Hinkle, *Mechanical Vibrations* (Allyn and Bacon, 1978), Chap. 7.

²⁵M. P. Païadoussis and G. X. Li, *J. Fluids Struct.* **7**, 137 (1993).

²⁶V. Sazonova, Ph.D. thesis, Cornell University, 2006.

²⁷See, for example, Frank S. Crawford, Jr., *Berkeley Physics Course: Waves* (McGraw-Hill, New York, 1968), p. 4.

²⁸unpublished data on carbon nanotube from our group.

²⁹<http://www.knovel.com> (search for SiC, go to Physical Properties of Semiconductors, then Young's Modulus, Poisson Ration and Similar).

³⁰<http://www.memstnet.org/material/siliconcarbidesic>

³¹http://www.allmeasures.com/Formulae/static/materials/159/youngs_modulus.htm

³²<http://www.ioffe.ru/SVA/NSM//Semicond/SiC/mechanic.html>

³³*Gmelins Handbuch der Anorganischen Chemie: Silicium*, 8th ed. (Chemie GmbH, Weinheim, 1959), Pt. B.

³⁴E. W. Wong, P. E. Sheehan, and C. M. Lieber, *Science* **277**, 1971

- (1997).
- ³⁵G. L. Harris, in *Properties of Silicon Carbide*, EMIS Data-reviews Series No. 13, edited by G. L. Harris (Institution of Engineering and Technology, London, 1995), p. 8.
- ³⁶X. Chen, S. Zhang, G. J. Wagner, W. Ding, and R. S. Ruoff, *J. Appl. Phys.* **95**, 4823 (2004).
- ³⁷X. L. Feng, C. A. Zorman, M. Mehregany, and M. L. Roukes, Solid-State Sensors, Actuators, and Microsystems Workshop, Hilton Head Island, 4–8 June 2006 (unpublished).
- ³⁸M. D. LaHaye, O. Buu, B. Camarota, and K. C. Schwab, *Science* **304**, 74 (2004).
- ³⁹K. Schwab, *Appl. Phys. Lett.* **80**, 1276 (2002).
- ⁴⁰A. B. Hutchinson, P. A. Truitt, K. C. Schwab, L. Sekaric, J. M. Parpia, H. G. Craighead, and J. E. Butler, *Appl. Phys. Lett.* **84**, 972 (2004).
- ⁴¹A. N. Cleland and M. L. Roukes, *Appl. Phys. Lett.* **69**, 2653 (1996).
- ⁴²D. W. Carr, S. Evoy, L. Sekaric, H. G. Craighead, and J. M. Parpia, *Appl. Phys. Lett.* **75**, 920 (1999).
- ⁴³G. M. Kim, S. Kawai, M. Nagashio, H. Kawakatsu, and J. Brugger, *J. Vac. Sci. Technol. B* **22**, 1658 (2004).